The effect of leg compliance in multi-directional jumping of a flea-inspired mechanism

2017 Bioinspir. Biomim. 12 026006

(http://iopscience.iop.org/1748-3190/12/2/026006)

Bioinspiration & Biomimetics

PAPER

The effect of leg compliance in multi-directional jumping of a flea-inspired mechanism

RECEIVED
10 August 2016

REVISED
3 January 2017

ACCEPTED FOR PUBLICATION
6 January 2017

PUBLISHED
10 February 2017

Gwang-Pil Jung[1], Hong-Cheol Choi[2] and Kyu-Jin Cho[1]

[1] School of Mechanical and Aerospace Engineering/Institute of Advanced Machines and Design, Seoul National University, Seoul 151-742, Republic of Korea

[2] Department of Physics and Chemistry, Korea Military Academy, Seoul, Republic of Korea

E-mail: kjcho@snu.ac.kr

Keywords: jumping robot, compliant leg, conversion efficiency

Abstract

Inspired by the relationship between leg compliance and jumping performance in the false stick insect, this paper describes how variations in leg compliance and jumping direction affect the performance of a flea-inspired jumping mechanism. The amount of energy lost during jumping was determined by examining the ratio of kinetic energy to input energy (also called conversion efficiency). Leg compliance is modeled based on the compliant mechanics to determine energy transfer during jumping and determined the optimum degree of leg compliance for maximizing performance. Jumping experiments are then performed using six different legs with progressively greater degrees of stiffness and three different jumping directions. The experiments show that conversion efficiency decreases by approximately 3–5% as leg stiffness increases, compared to the optimal case. In the most compliant legs (i.e. stiffness of 0.0338 Nm rad^{-1} or less), conversion efficiency rapidly drops to near 0% because the leg bends so much that it cannot support the thrusting force. The optimal conversion efficiency tends to increase when the mechanism jumps vertically owing to reduced slippage and increased ground reaction force. These investigations show that optimizing leg compliance can improve the performance of a jumping robot by up to 5% by enabling more of the initially stored energy in the leg to be used. This finding will likely prove helpful for choosing the leg stiffness for a small-scale jumping robot.

1. Introduction

Leg compliance is a key factor in the running and jumping performance of legged locomotors. Legged animals achieve robust and stable running locomotion by actively controlling their effective leg compliance through the coordination of their muscles, ligaments, and tendons to suit the conditions of surface compliance and payload (Ferris *et al* 1998, Full *et al* 2000). Biomechanical studies of animals have provided insights on applying the concept of leg compliance to the design of legged robotic systems.

Empirical studies on running robots have illuminated the relationship between leg stiffness and leg compliance. Raibert *et al* first suggested a mechanically tunable leg for a dynamic locomotor that uses an air spring and serially connected hydraulic actuators to control leg stiffness (Raibert *et al* 1989). They concluded that a leg with high stiffness enabled the robot to run faster. Hurst *et al* studied the role of compliance in legged locomotion using an actuator with mechanically tunable series compliance (Hurst *et al* 2010) and found that tuning spring stiffness increased the energy efficiency of their robot's gaits. Galloway *et al* gave their hexapedal robot, EduBot, a leg design with tunable stiffness (Galloway *et al* 2009, 2011) and performed running experiments varying leg stiffness, surface compliance, and payload that revealed the existence of an optimal leg stiffness that could increase running speed and efficiency.

The stick insect stores most of the elastic energy in stiff cuticular parts having large modulus compared to muscle, which enables amplifying the power and releasing the stored energy much faster. Muscle contraction causes little deformation of the chitinous cuticle and store the energy needed for jumping. After that, the stored energy is released in several milli seconds. During the process, the stick insect shows considerable bending of the hind-leg tibiae due to the compression in the acceleration phase. The stick insect stores about 7%

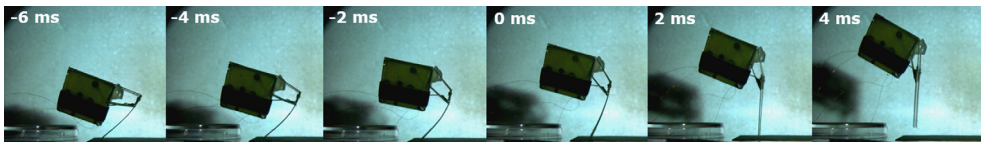

Figure 1. The flea-inspired jumping mechanism takes off with its leg being bent (Noh *et al* 2012).

of the total jumping energy in its bent tibiae and releases the stored energy before take-off. At the moment of take-off, however, some of the stored energy still remain in the tibiae since the tibiae are not fully straightened.

In jumping robots, a similar leg bending phenomenon can be found (Noh *et al* 2012, Koh *et al* 2015). Many milli-scale mobile robots have been designed with jumping legs, because jumping locomotion helps to overcome these robots' size limitations by extending their range and enabling them to overcome large obstacles. To make this possible, researchers have employed various energy storing and releasing methods including an escapement mechanism (Kovac *et al* 2008, Nguyen and Park 2012, Vidyasagar *et al* 2015), one-way bearing (Zhao *et al* 2013), chemical energy (Tolley *et al* 2014), torque reversal (Koh *et al* 2015, Jung and Cho 2016), an active clutch (Desbiens *et al* 2014, Zaitsev *et al* 2015, Jung *et al* 2016), and power modulation (Haldane *et al* 2016). Small jumping robots thereby have the potential for use in inspection, surveillance, and disaster relief applications, which can pose dangers to humans. To attain a high take-off velocity and enhanced maneuverability, jumping robots initially store energy in an elastic component, and release the stored energy all at once. Due to this bursting motion, these robots experience high rates of acceleration, up to orders of magnitude greater than the gravitational acceleration $-500\ \mathrm{m\ s^{-2}}$ for the jumping mechanism in this paper. The resulting large compression load is exerted on the jumping legs, resulting in bending. As far as we can tell, no studies have been performed that observe how bending effects the locomotion on a jumping robot's legs.

Inspired by the false stick insect's jumping, we have investigated how leg bending affects jumping performance by studying a flea-inspired jumping mechanism, a milli-scale robot proposed by our research group in 2012 (Noh *et al* 2012) (see figure 1). Both jumping mechanisms from the false stick insect and the flea-inspired mechanism go through high compression loading during acceleration, inducing a bending in the legs. Compression loads of ~400 mN is exerted on the jumping legs of the flea-inspired mechanism (about twenty times of its body weight), and ~46 mN is exerted on the false stick insect's legs (about three times of its body weight) (Burrows and Wolf 2002). Although there is a difference in the magnitude between both compression load cases, the basic principle, compression induced bending, is equally true in both jumping leg cases.

We previously examined the effect of leg compliance on the performance of this mechanism when jumping in a single direction (Kim *et al* 2013a, Jung *et al* 2014) and concluded that the greatest amount of the initially stored energy can be converted to kinetic energy when the leg exhibits optimal compliance. In this paper, we extend this earlier study to investigate how leg compliance affects performance of the mechanism when it jumps in multiple directions. To evaluate performance and efficiency, we examine the concept of conversion efficiency, which deals with the ratio of kinetic energy to initially stored energy (Burdick and Fiorini 2003). To precisely calculate conversion efficiency, a dynamic model based on compliant mechanics is developed and energy distribution at the moment of take-off is analyzed. Using this model, five types of transferred energy are investigated: potential, rotational kinetic, translational kinetic, vibrational, and residual energy (i.e. the unconverted portion of the initially stored energy). Jumping experiments are performed by varying leg stiffnesses and three different initial launch angles (42°, 54°, and 70°) to check the effect of leg compliance when the mechanism jumps in multiple directions. The modeling and experimental results demonstrate how optimal compliance changes according to the initial launch angle.

The paper is organized as follows: section 2 describes the bioinspiration for this work in the way that the false stick insect bends its tibiae when it jumps. Section 3 presents a dynamic model of leg compliance based on the pseudo-rigid-body model. Section 4 describes fabrication and assembly of the experimental mechanism, and section 5 describes experimental observations of the effect of leg compliance, in terms of leg stiffness and launch angle, on the mechanism's jumping performance.

2. Leg bending in the false stick insect

The false stick insect can jump and kick rapidly and powerfully like a locust. During take-off, the hind tibiae of its jumping legs undergo considerable compression load owing to high acceleration (about $165\ \mathrm{m\ s^{-2}}$ (Burrows and Wolf 2002)), which results in bending of the tibiae. Figure 2 schematically shows the jumping process of the false stick insect. The insect jumps using its long, thin hind legs. During a jump, the hind tibiae bend owing to a compression load of about 23 mN. The distance that shows the degree of bending is maximized in the acceleration phase, as shown in figure 2. According to (Burrows and Wolf 2002), the maximum distance is 3.5 mm, which is twice the natural state value of 1.7 mm.

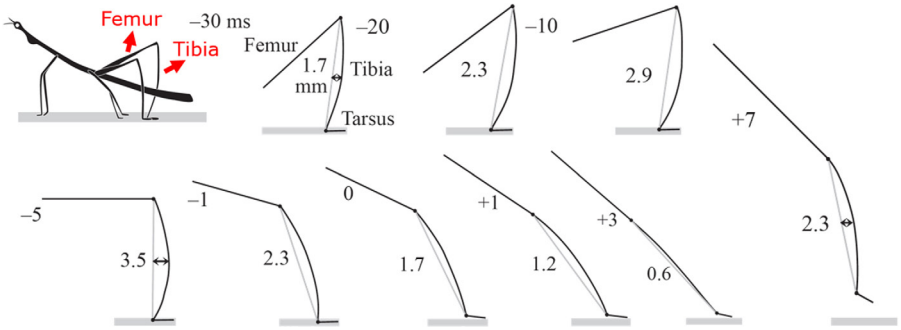

Figure 2. The hind tibiae bend when a false stick insect jumps (adapted from Burrows *et al* (2002) and Burrows and Wolf (2002)). Reproduced with permission from Burrows and Wolf, copyright 2002 Company of Biologists.

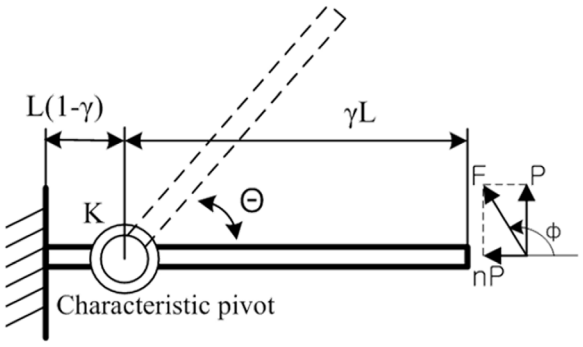

Figure 3. PRBM model of the compliant leg (Howell 2001). The origin is located at the point where the reaction forces are exerted.

Table 1. PRBM parameters.

Direction of reaction force, n	Characteristic radius factor, γ	Max. pseudo-rigid-body angle, Θmax(deg)	Stiffness coefficient, K_θ
2	0.8276	69	2.597 07

One notable observation is that the hind tibiae repeat the bending and unbending motions after take-off. Given that the hind tibiae do not experience any external load after take-off, this vibration must be caused by the fact that the false stick insect jumps with bent hind tibiae. Therefore, bending and unbending of the hind tibiae is repeated even after take-off. This may seem inefficient in that the energy left in the bent tibiae is definitely exhausted as vibrational energy.

Our flea-inspired jumping mechanism also performs take-off with bent legs, as shown in figure 1. The legs maximally bend in the acceleration phase, and when take-off happens, the legs remain bent (0 ms in figure 1). After take-off, bending and unbending of the jumping legs repeats for a while, then reduces gradually owing to damping of the legs.

3. Leg compliance modeling

To examine how stored energy transfers during jumping, leg compliance needs to be modeled. However, it is challenging to apply linear beam theory to this case because the leg of the flea-inspired mechanism undergoes significant deflection when the mechanism takes off, as shown in figure 1. The extent of this deflection further increases when the mechanism's legs are highly compliant.

The pseudo rigid body model (PRBM) is used (Howell 2001, Su 2009) to describe large beam deflections. The PRBM allows analysis of a beam undergoing large deflection by describing the beam as a series of multiple rigid beams connected by flexural pivots, according to the loading condition.

3.1. Bending leg

The modeling of a compliant beam differs according to the loading condition. In this case, one end of the leg is fixed to a four-bar mechanism and the other is freely loaded; therefore, the jumping leg is regarded as a cantilevered segment with forces at the free end. In figure 3, two rigid links and a joint having a torsional spring describe the compliant leg.

After segmenting the compliant beam, the location and stiffness of the torsional spring are determined based on a particular loading condition with load direction, n, and the maximum pseudo-rigid-body angle, Θ_{max}. According to the reaction force curve shown in previous research, parameters such as the characteristic radius factor, γ, and the stiffness coefficient,

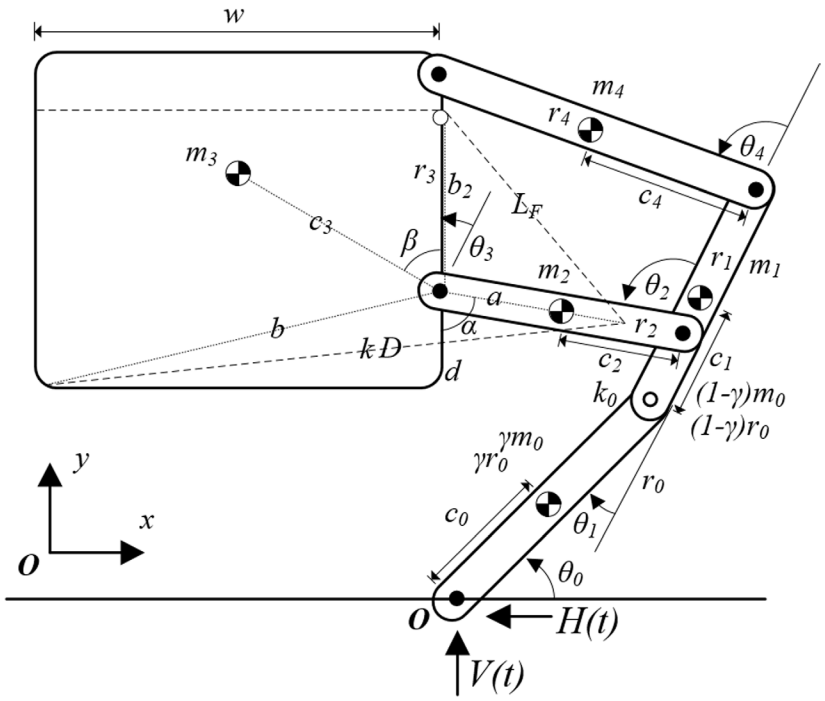

Figure 4. Parameters used to model the compliant leg with PRBM.

K_θ, are determined as indicated in table 1. The stiffness of the torsional spring is given as $k = \gamma K_\theta EI/L$, where E is Young's modulus, I is the moment of inertia, and L is the length of the compliant leg.

3.2. Take-off

As shown in figure 4, five rigid links and six rotational joints describe the jumping mechanism and its compliant leg. To express the jumping motion, five parameters, θ_0, θ_1, θ_2, θ_3, and θ_4, are employed to show the position, P_i, of each link.

$$P_0 = \begin{pmatrix} c_0 \cos\theta_0 \\ c_0 \sin\theta_0 \end{pmatrix} \tag{1}$$

$$P_1 = \begin{pmatrix} \gamma r_0 \cos\theta_0 + c_1 \cos(\theta_0 + \theta_1) \\ \gamma r_0 \sin\theta_0 + c_1 \sin(\theta_0 + \theta_1) \end{pmatrix} \tag{2}$$

$$P_2 = \begin{pmatrix} \gamma r_0 \cos\theta_0 + (1-\gamma) r_0 \cos(\theta_0 + \theta_1) \\ \quad + c_2 \cos(\theta_0 + \theta_1 + \theta_2) \\ \gamma r_0 \sin\theta_0 + (1-\gamma) r_0 \sin(\theta_0 + \theta_1) \\ \quad + c_2 \sin(\theta_0 + \theta_1 + \theta_2) \end{pmatrix} \tag{3}$$

$$P_3 = \begin{pmatrix} \gamma r_0 \cos\theta_0 + (1-\gamma) r_0 \cos(\theta_0 + \theta_1) \\ \quad + r_2 \cos(\theta_0 + \theta_1 + \theta_2) \\ \quad + c_3 \cos(\theta_0 + \theta_1 + \theta_2 + \beta) \\ \gamma r_0 \sin\theta_0 + (1-\gamma) r_0 \sin(\theta_0 + \theta_1) \\ \quad + r_2 \sin(\theta_0 + \theta_1 + \theta_2) \\ \quad + c_3 \sin(\theta_0 + \theta_1 + \theta_2 + \beta) \end{pmatrix} \tag{4}$$

$$P_4 = \begin{pmatrix} \gamma r_0 \cos\theta_0 + ((1-\gamma) r_0 + r_1) \cos(\theta_0 + \theta_1) \\ \quad + c_4 \cos(\theta_0 + \theta_1 + \theta_4) \\ \gamma r_0 \sin\theta_0 + ((1-\gamma) r_0 + r_1) \sin(\theta_0 + \theta_1) \\ \quad + c_4 \sin(\theta_0 + \theta_1 + \theta_4) \end{pmatrix} \tag{5}$$

where r_i is the length of each link, c_i is the distance between the center of mass of each link and the adjacent joint, and β is the angle between r_3 and c_3.

In total, the mechanism has three degrees of freedom and the generalized coordinates θ_0, θ_1, and θ_2. Other parameters, such as θ_3, θ_4, are indicated based on the following kinematic relationship of the four-bar mechanism.

$$r_1 - r_4 \cos\theta_3 = r_2 \cos\theta_2 + r_3 \cos\theta_4 \tag{6}$$

$$r_4 \sin\theta_3 = r_2 \sin\theta_2 + r_3 \sin\theta_4 \tag{7}$$

Based on these positions and the kinematic constraints, the dynamics of jumping may be numerically calculated by a Lagrange formulation.

$$L = T - V \tag{8}$$

$$T = \frac{1}{2} \sum_{i=0}^{4} m_i v_i^2 \tag{9}$$

$$V = \sum_{i=0}^{4} m_i g P_{i,y} + \frac{1}{2} k (D - D_0)^2 + \frac{1}{2} k_0 \theta_1^2 \tag{10}$$

where L is the Lagrangian for the system, T is the total kinetic energy, V is the total potential energy, g is the gravitational acceleration, $P_{i,y}$ is the vertical position of each link, k is the extensor spring constant, k_0 is the

Table 2. Material properties of the fabricated legs.

Sample No.	Material	Number of layers	Thickness (mm)	Width (mm)	Length (mm)	Young's modulus (Gpa)	Mass (g)	Bending stiffness[a] (Nm rad^{-1})
1	GFRP	3	0.15	6	19.5	13.3929	0.028	0.0108
2	GFRP	6	0.27	6	19.5	7.2056	0.038	0.0338
3	GFRP	10	0.39	6	19.5	7.3547	0.068	0.0496
4	GFRP	8	0.28	6	19.5	11.4654	0.049	0.0620
5	GFRP	21	0.64	2	19.5	7.3312	0.084	0.0868
6	GFRP	21	0.64	6	19.5	7.3058	0.092	0.2576

[a] Bending stiffness is for a pair of jumping legs, so these values are twice those of a single jumping leg.

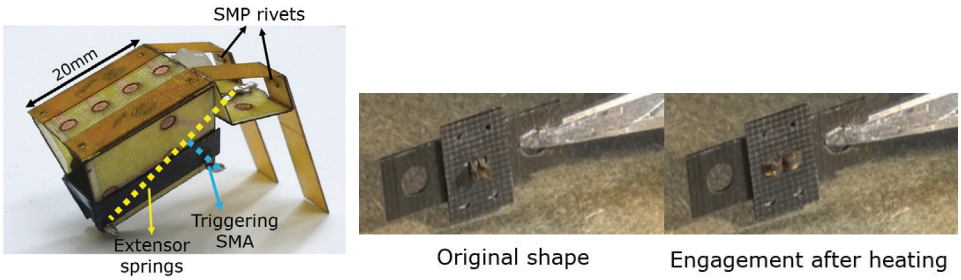

Figure 5. (a) The assembled flea-inspired jumping mechanism, showing sample leg 4. The black-colored rectangle on the body is the stiffener that reinforces the body, consisting of 6 layers of cured carbon fiber. (b) The SMP rivet fastener operates by heating.

torsional spring constant in the jumping leg, D is the current length of the extensor spring, and D_0 is the initial length of the extensor spring.

The derived Lagrangian of the system satisfies the following Euler–Lagrangian equation with an assumption that considers conservative forces.

$$\frac{\mathrm{d}}{\mathrm{d}t}\left(\frac{\partial L}{\partial \dot{\theta}_i}\right) - \frac{\partial L}{\partial \theta_i} = 0, \quad i = 0,\ 1,\ 2 \tag{11}$$

The generalized coordinates have the following initial conditions:

$$\theta_0 = 48°,\ 58° \text{ and } 73\,° \tag{12}$$

$$\theta_1 = 0\,° \tag{13}$$

$$\theta_2 = 126.05\,° \tag{14}$$

where θ_0 is the launch angle, θ_1 is the initial bending angle of the jumping leg, and θ_2 is the angle that determines the orientation of the four-bar transmission. Note that the value of θ_2 is set to simulate the state just before take-off.

The jumping mechanism takes off when the vertical reaction force, $V(t)$, is zero. The reaction forces in the x and y directions are given as follows:

$$m_{\text{robot}} a_{\text{robot},x} = \sum_{i=0}^{4} m_i a_{i,x}(t) = -H(t) \tag{15}$$

$$m_{\text{robot}} a_{\text{robot},y} = \sum_{i=0}^{4} m_i a_{i,y}(t) = V(t) - \sum_{i=0}^{4} m_i g \tag{16}$$

where m_{robot} is the total mass of the robot, a_{robot} is the acceleration of the center of mass, a_i is the acceleration of each link, and H is the horizontal reaction force on the ground. Equations (17) and (18) indicate the angular and translational velocities during take-off, respectively.

$$m_{\text{robot}} w_{\text{robot}} = \sum_{i=0}^{4} m_i w_{i,f} \tag{17}$$

$$m_{\text{robot}} v_{\text{robot}} = \sum_{i=0}^{4} m_i v_{i,f} \tag{18}$$

where v_{robot} is the velocity of the center of mass and w_{robot} is the angular velocity of the robot. $v_{i,f}$ and $w_{i,f}$ are the translational velocity and angular velocity of each link just before take-off.

4. Fabrication and assembly

Six jumping legs having different stiffnesses are studied in the jumping experiments. Table 2 lists their material properties. Young's modulus is determined based on the three-point bending test. Bending stiffness, k, is calculated using the measurements of E in the relation, $k = \gamma K_\theta EI/L$. 60 μm glass fiber prepreg (Real Carbon, Inc.) is used to make the jumping legs. Leg stiffness is adjusted by varying the number of stacking layers (see table 2) and using different hardeners (Kukdo Chemical). G-0240 hardener is used to make samples 1 and 4, and G-A0533 hardener is used for the rest of the

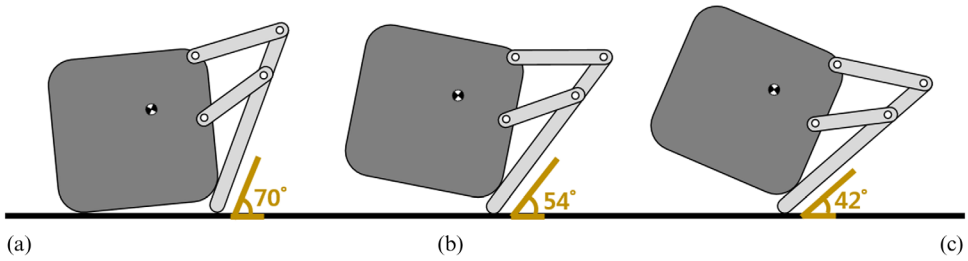

Figure 6. Depiction of the selected launch angles of (a) 70°, (b) 54°, and (c) 42°.

samples. The flexural stiffness of G-0240 is about 1.7 times larger than that of G-A0533.

The same jumping mechanism body is used in all of the jumping tests to ensure that the extensor had the same amount of initially stored energy for each experiment. To enable the legs to be changed out easily without being damaged, we employ shape memory polymer (SMP) rivet fasteners, shown in figure 5(a) (Kim *et al* 2013b). SMP recovers its shape and alters the modulus in response to temperature changes (figure 5(b)). Thanks to these properties, SMP rivet fasteners are reversibly usable and possess sufficient disengagement force (up to 7 N) despite their lightweight mass (0.003 g). Simple I-beam-shaped SMP rivet fasteners are designed and installed through a hole inside the four-bar mechanism shown in figure 5(a) (Kim *et al* 2013a).

To store elastic energy, two linear springs are used as extensors. They are installed inside the body of the mechanism. The extensors have a spring coefficient of 280 N m^{-1}. A shape memory alloy (SMA) actuator is used to trigger jumping. When the SMA actuator is heated, its phase changes to the austenite phase and the SMA actuator contracts, triggering the mechanism (Otsuka and Wayman 1999). Also, to prevent deformation caused by repeated experiments, six layers of carbon fiber prepreg reinforce the flea body, as shown in figure 5(a).

5. Experimental and simulated results

To examine how leg compliance and jumping direction affect jumping performance, experiments are performed with the flea-inspired mechanism, using six legs of different stiffnesses (see table 2) and three different initial launch angles (42°, 54°, and 70°; see figure 6).

Experimentally evaluating the conversion efficiency of the mechanism at take-off is challenging because the extensor is installed inside the body, which prevents observation of the energy remaining in the extensor, even with a high-speed camera. To determine the precise conversion efficiency, energy transfer was analyzed using the dynamic model with validation.

At a launch angle of 42°, the mechanism's body is the closest to the vertical. When the launch angle is smaller than 42°, the robot falls backward. The launch angle of 70° is the maximum angle that satisfies geometric constraints, and at this angle the initial posture of the body is the closest to the horizontal. Jumping at all three launch angles is recorded three times via a high-speed camera with a frame rate of 5000 fps. A video analysis tool (ProAnalyst) is used to analyze the data, and a first-order low-pass filter is applied to the data with a 270 Hz cutoff frequency. Based on this process, the velocity and translational kinetic energy at take-off are determined.

5.1. Simulated results

Simulations are performed until the reaction force in the vertical direction reached zero, which means the moment of take-off. Figure 7 shows the acceleration, the ground reaction force and the visualization of the mechanism during the simulation. Figure 7(a) shows the results obtained using the leg with the lowest stiffness (0.0108 N m^{-1}), figure 7(b) shows the results obtained using a leg with an intermediate level of stiffness (0.0496 Nm rad^{-1}), and figure 7(c) shows the results obtained using the leg with the highest stiffness (0.2576 Nm rad^{-1}).

The major difference between the more compliant and less compliant leg models is the amount of vibration in the jumping leg. Figure 7 (left column) shows that the frequency of the leg vibration during jumping increased as leg stiffness increased, following the natural frequency. Based on this model, the energy conversion from the initially stored energy to leg vibrational energy is calculated.

Figure 9 (right column) shows the take-off velocity of the model and the experimental results obtained by varying leg stiffness and launch angles. Overall, the data peak near the bending stiffness of 0.05 Nm rad^{-1} and converge as the stiffness increases. As the launch angle increases, however, the velocity data show a mismatch between the simulated and the experimental results. In the case of the 70° launch angle, and especially in the x direction, the velocity data shown in figure 9(a) (left column) greatly deviate from the simulated data. The jumping error that occurs with this large launch angle is caused by slippage during take-off, as shown in figure 10 (left column). In our dynamic model, the contact point between the leg and the ground is described as a rotational joint and slippage is hardly considered, which introduces this discrepancy between the simulated and the experimental results.

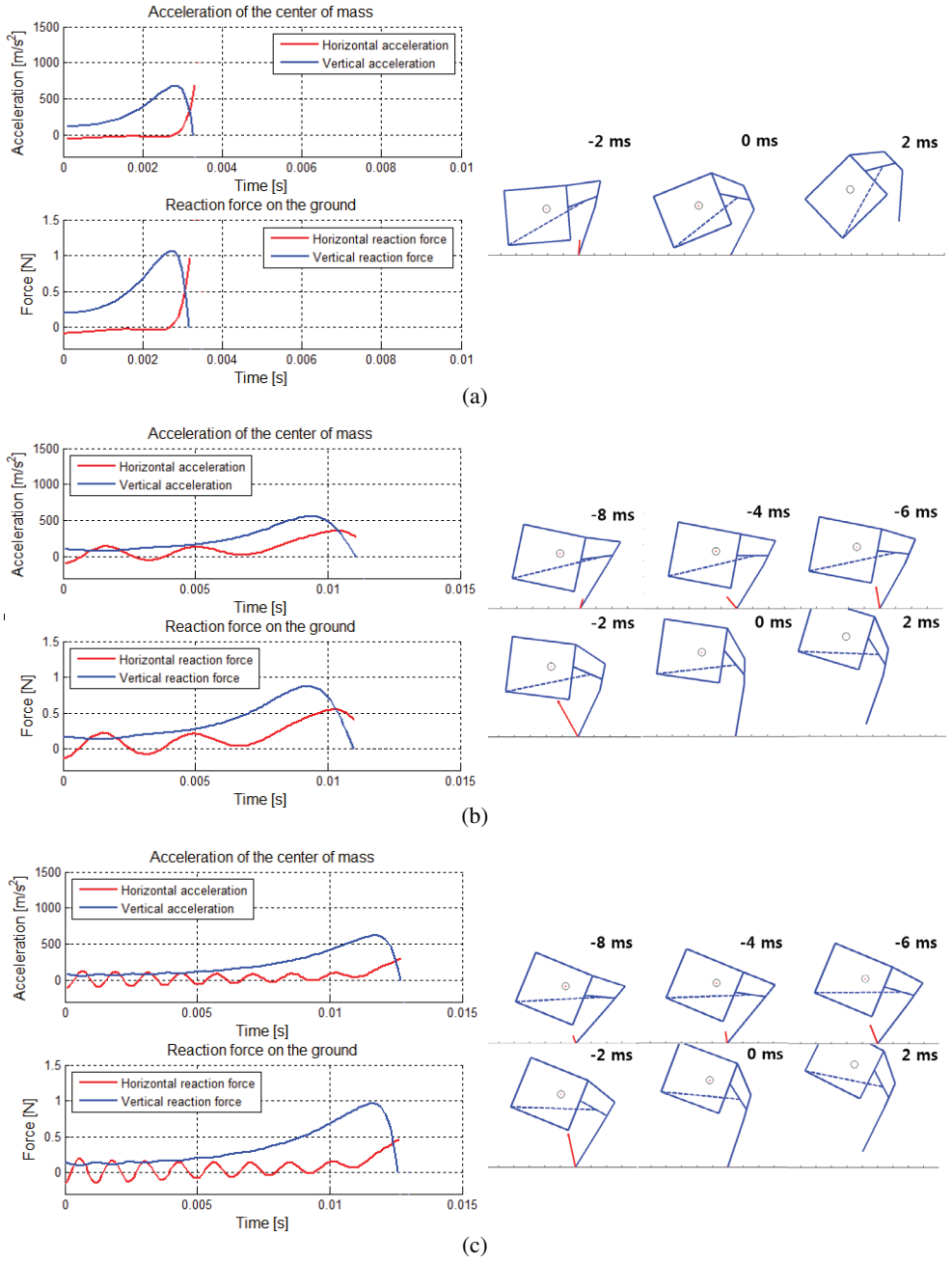

Figure 7. Modeling data for acceleration and ground reaction force and visualization of the corresponding jumping sequence of the model. (a) Leg stiffness of 0.0108 Nm rad^{-1} (70° initial angle). (b) Leg stiffness of 0.0496 Nm rad^{-1} (54° initial angle). (c) Leg stiffness of 0.2576 Nm rad^{-1} (42° initial angle). The red arrows indicate a vector of the ground reaction force, and the circle in the body indicates the center of mass. Also, the visualized model reflects the take-off velocity after take-off, maintaining the configuration of the mechanism.

The discrepancy tends to be large during jumping at large launch angles, and this can be described by the reduced normal force and correspondingly insufficient friction. In the simulated reaction force plots in figure 7 (left column) and the measured reaction force plot in figure 8, the vertical reaction force decreases while the horizontal reaction force greatly increases at a launch angle of 70°. This phenomenon causes insufficient friction to be provided during take-off, and slippage is more likely to occur when the mechanism jumps horizontally. At a launch angle of 42°, however, the simulated and experimental results match quite well because the vertical reaction force provides sufficient friction and slippage hardly occurs.

5.2. Energy distribution at take-off

The conversion efficiency of the jumping mechanism is determined by investigating energy distribution at take-off both experimentally and via simulation. When the mechanism takes off, the energy initially stored in the extensor transfers to translational kinetic energy, rotational kinetic energy, and vibrational energy of the leg. Additionally, there is residual energy in the extensor, meaning the unconverted portion of the initially

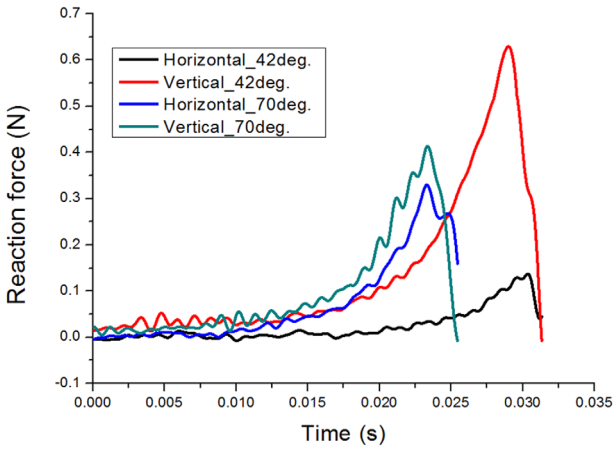

Figure 8. Measured ground reaction force for a leg stiffness of 0.0496 Nm rad^{-1} and launch angles of 42° and 70°.

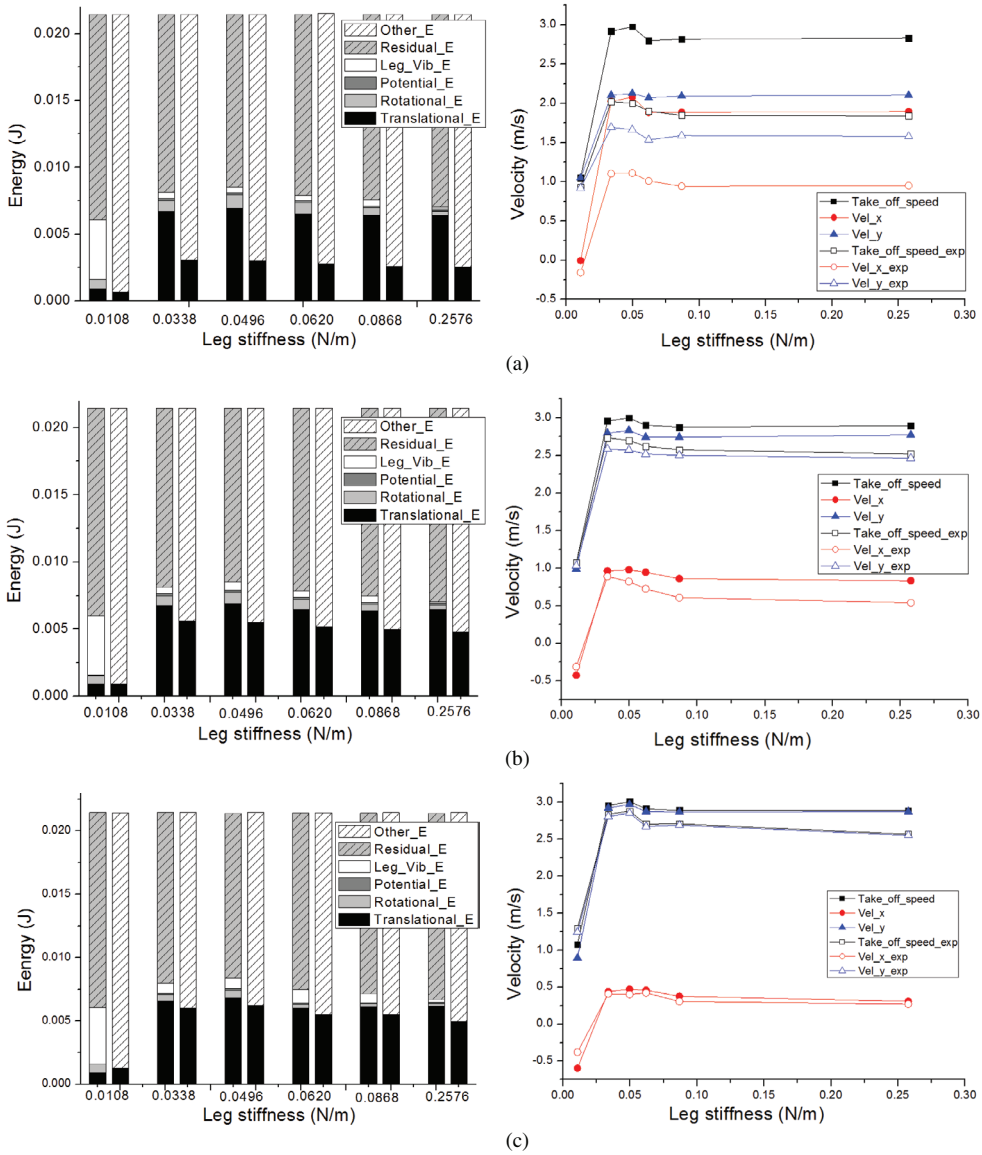

Figure 9. Energy distribution at take-off (left) and take-off velocity (right) with launch angles of (a) 70°, (b) 54°, and (c) 42°. Note that the bars with bold border line represent the experimental data. The experiment measured only translational kinetic energy because of the difficulty of measuring the other energies.

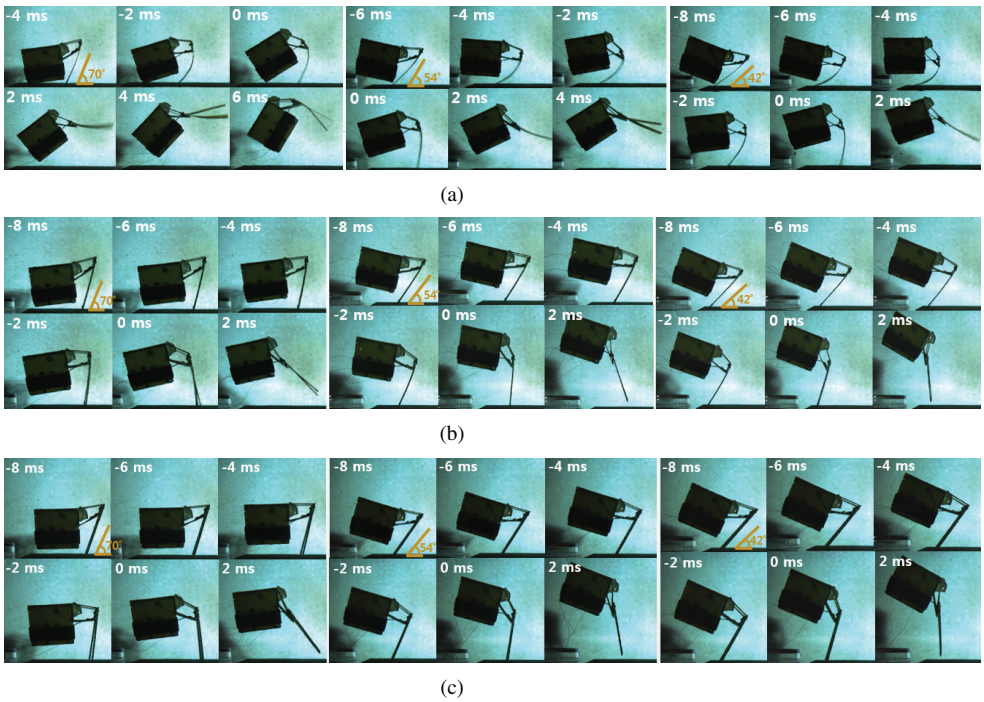

Figure 10. Leg bending during take-off with a leg stiffness of (a) 0.0108 N m^{-1}, (b) 0.0496 N m^{-1}, and (c) 0.0868 N m^{-1}. Lauch angles are 70° (left column), 54° (middle column), and 42° (right column). Note that the initial orientation of launch angles is indicated with orange-colored lines.

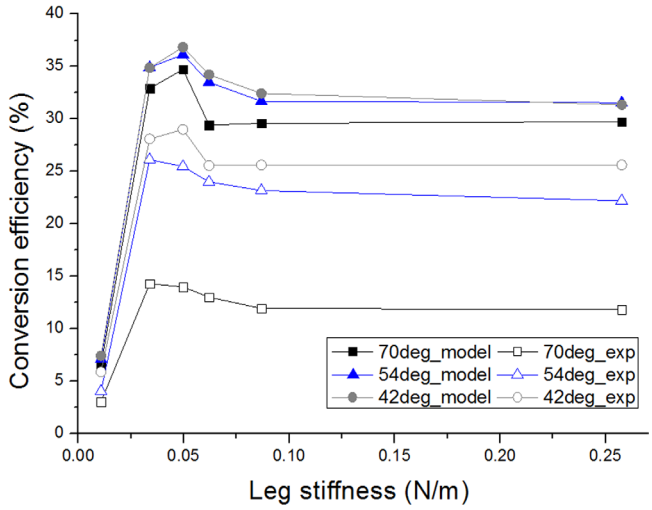

Figure 11. Conversion efficiency as a function of the stiffness of the jumping legs.

stored energy. Figure 9 (left column) shows the energy distribution at take-off. This figure provides only results for translational kinetic energy. The other four types of energy are specified as 'other energy' owing to the difficulty of measuring them.

Both leg vibrational energy and residual energy in the extensor worsen conversion efficiency, varying with leg stiffness. The leg vibrational energy increases as leg compliance increases. This phenomenon is shown in figure 10. When leg stiffness is 0.0108 N m^{-1}, the compliant leg bends greatly at all launch angles (figure 10(a)) when the mechanism takes off. In the energy distribution plots in figure 9 (left column), stored energy increasingly converts to leg vibrational energy as leg stiffness decreases.

Somewhat different behavior is shown in case of residual energy. The amount of residual energy drops as stiffness decreases to 0.0496 Nm rad^{-1}, as shown in figure 9 (left column). Over this range, the initially stored energy is increasingly converted to kinetic and vibrational energy as leg stiffness decreases. In the most compliant case (leg stiffness of 0.018), however, the residual energy itself stiffly increases, meaning that the mechanism jumps before energy transfer finishes and thus prematurely leaves the ground (Fiorini and Burdick 2003).

5.3. Conversion efficiency as a function of launch angle

In the simulated results, the optimal leg stiffness for maximizing conversion efficiency is 0.0496 Nm rad^{-1}, and that value does not change as launch angle varies. In the experimental results, however, the optimal leg stiffness tends to increase as the mechanism jumps vertically, as shown in figure 11, which shows that for the 70° and 54° launch angles, conversion efficiency is maximized at the leg stiffness of 0.0338 Nm rad^{-1}. When the launch angle is 42°, conversion efficiency is maximized at the leg stiffness of 0.0496 Nm rad^{-1}.

This difference originates in the different external loads exerted on the jumping legs at each launch angle. Our model does not reflect slippage, and therefore the external load (i.e. the ground reaction force) required to induce bending of the jumping legs does not vary. Our experiments, however, showed that the ground reaction force decreases greatly as the mechanism launches horizontally. Figure 8 shows that the maximum vertical reaction force (which compresses the leg) reduces when the mechanism jumps horizontally. Accordingly, less load is exerted on the legs, and a relatively low level of leg stiffness is sufficient to support jumping.

6. Conclusion

During take-off, the false stick insect goes through high acceleration that is up to an order of magnitude greater than the gravitational acceleration. The resulting large compression load and bending moment cause its hind tibiae to bend considerably. We were inspired by this phenomenon to investigate how bending in the legs of a milli-scale flea-inspired jumping mechanism affects its jumping performance. To judge jumping performance, the effect of jumping direction and leg stiffness on conversion efficiency was examined. To precisely derive conversion efficiency, we developed a dynamic PRBM model and analyzed energy transfer during jumping in order to determine the optimal leg stiffness for minimizing the vibrational energy of the jumping leg while maximizing the kinetic energy from the initially stored energy. The model predicted that the optimal compliance increases as the direction of jumping becomes more vertical owing to reduced slippage and an increased ground reaction force. In terms of leg stiffness, conversion efficiency decreases by approximately 3–5% as leg stiffness increases, compared to the optimal case. When the leg highly compliant (i.e. leg stiffness of 0.0338 and 0.018 Nm rad^{-1}), conversion efficiency rapidly drops to near zero because the leg is bending too much to support the thrusting force.

We believe that this investigation will provide helpful guidance for the design of small-scale jumping robots. Our findings show that leg stiffness influences jumping performance. If precise dynamic modeling and simulation are possible, we recommend analysis to determine the optimal leg stiffness because designing around this value can increase jumping performance by up to 5%. If the robot is too complex to be modeled, then the design should take account of our finding that a relatively stiff leg provides better performance than a compliant one because conversion efficiency has the potential to drop rapidly if leg stiffness is below the optimal value. Generally speaking, using a rigid leg would be a safe way to improve the performance of a jumping robot.

Acknowledgment

The authors thank to Wooyoung Kim and Prof Frank C Park for the constructive comments and discussions. This research was supported by a grant to the Bio-Mimetic Robot Research Center, funded by the Defense Acquisition Program Administration under the grant number UD130070ID.

References

Burdick J and Fiorini P 2003 Minimalist jumping robots for celestial exploration *Int. J. Robot. Res.* **22** 653–74

Burrows M and Wolf H 2002 Jumping and kicking in the false stick insect Prosarthria teretrirostrix kinematics and motor control *J. Exp. Biol.* **205** 1519–30

Desbiens A L, Pope M T, Christensen D L, Hawkes E W and Cutkosky M R 2014 Design principles for efficient, repeated jumpgliding *Bioinspir. Biomim.* **9** 025009

Ferris D P, Louie M and Farley C T 1998 Running in the real world: adjusting leg stiffness for different surfaces *Proc. R. Soc.* B **265** 989–94

Fiorini P and Burdick J 2003 The development of hopping capabilities for small robots *Auton. Robots* **14** 239–54

Full R J, Farley C T and Winters J M 2000 *Biomechanics and Neural Control of Posture and Movement* (Berlin: Springer) pp 192–205

Galloway K C, Clark J E and Koditschek D E 2009 Design of a tunable stiffness composite leg for dynamic locomotion *ASME 2009 Int. Design Engineering Technical Conf. and Computers and Information in Engineering Conf.* (American Society of Mechanical Engineers) pp 215–22

Galloway K C, Clark J E, Yim M and Koditschek D E 2011 Experimental investigations into the role of passive variable compliant legs for dynamic robot locomotion *IEEE Int. Conf. on Robotics and Automation (ICRA)*

Haldane D W, Plecnik M, Yim J and Fearing R 2016 Robotic vertical jumping agility via series-elastic power modulation *Sci. Robot.* **1** eaag2048

Howell L L 2001 *Compliant Mechanisms* (New York: Wiley)

Hurst J W, Chestnutt J E and Rizzi A A 2010 The actuator with mechanically adjustable series compliance *IEEE Trans. Robot.* **26** 597–606

Jung G-P, Casarez C S, Jung S-P, Fearing R S and Cho K-J 2016 An integrated jumping-crawling robot using height-adjustable jumping module *IEEE Int. Conf. onRobotics and Automation (ICRA)* pp 4680–5

Jung G P and Cho K J 2016 Froghopper-inspired direction-changing concept for miniature jumping robots *Bioinspir. Biomim.* **11** 056015

Jung G P, Kim J S, Koh J S, Jung S P and Cho K J 2014 Role of compliant leg in the flea-inspired jumping mechanism *IEEE/RSJ Int. Conf. on Intelligent Robots and Systems (IROS)* pp 315–20

Kim J-S, Jung G-P, Koh J-S and Cho K-J 2013a Meso-scale robot assembly using shape memory polymer rivet fastener *2013 Int. Conf. on Intelligent Robots and Systems (IROS)* (IEEE) p 2082

Kim J-S, Lee D-Y, Koh J-S, Jung G-P and Cho K-J 2013b Component assembly with shape memory polymer fastener for microrobots *Smart Mater. Struct.* **23** 015011

Koh J-S, Yang E, Jung G-P, Jung S-P, Son J H, Lee S-I, Jablonski P G, Wood R J, Kim H-Y and Cho K-J 2015 Jumping on water: surface tension-dominated jumping of water striders and robotic insects *Science* **349** 517–21

Kovac M, Fuchs M, Guignard A, Zufferey J C and Floreano D 2008 A miniature 7g jumping robot *IEEE Int. Conf. on Robotics and Automation (ICRA)* pp 373–8

Nguyen Q-V and Park H C 2012 Design and demonstration of a locust-like jumping mechanism for small-scale robots *J. Bionic Eng.* **9** 271–81

Noh M, Kim S W, An S, Koh J S and Cho K J 2012 Flea-inspired catapult mechanism for miniature jumping robots *IEEE Trans. Robot.* **28** 1007–18

Otsuka K and Wayman C M 1999 *Shape Memory Materials* (Cambridge: Cambridge university press)

Raibert M H, Brown H B Jr, Chepponis M, Koechling J, Hodgins J K, Dustman D, Brennan W K, Barrett D S, Thompson C M and Hebert J D 1989 Dynamically stable legged locomotion (September 1985–1989) (Cambridge, MA: MIT)

Su H-J 2009 A pseudorigid-body 3R model for determining large deflection of cantilever beams subject to tip loads *J. Mech. Robot.* **1** 021008

Tolley M T, Shepherd R F, Karpelson M, Bartlett N W, Galloway K C, Wehner M, Nunes R, Whitesides G M and Wood R J 2014 An untethered jumping soft robot *IEEE/RSJ Int. Conf. on Intelligent Robots and Systems (IROS)* (IEEE) pp 561–6

Vidyasagar A, Zufferey J C, Floreano D and Kovac M 2015 Performance analysis of jump-gliding locomotion for miniature robotics *Bioinspir. Biomim.* **10** 025006

Zaitsev V, Gvirsman O, Ben Hanan U, Weiss A, Ayali A and Kosa G 2015 A locust-inspired miniature jumping robot *Bioinspir. Biomim.* **10** 066012

Zhao J, Xu J, Gao B, Xi N, Cintron F J, Mutka M W and Xiao L 2013 MSU jumper: a single-motor-actuated miniature steerable jumping robot *IEEE Trans. Robot.* **29** 602–14